PHYSICAL REVIEW E **92**, 052304 (2015)

Correlated two-particle diffusion in dense colloidal suspensions at early times: Theory and comparison to experiment

Zachary E. Dell,[1] Boyce Tsang,[1] Lingxiang Jiang,[2] Steve Granick,[1,2,3,4,*] and Kenneth S. Schweizer[2,3,†]
[1]*Department of Physics, University of Illinois, Urbana, Illinois 61801, USA*
[2]*Frederick Seitz Materials Research Laboratory, University of Illinois, Urbana, Illinois 61801, USA*
[3]*Department of Materials Science, University of Illinois, Urbana, Illinois 61801, USA*
[4]*IBS Center for Soft and Living Matter, Ulsan National Institute of Science and Technology, Ulju-gun 689-789, South Korea*
(Received 1 September 2015; published 6 November 2015)

The spatially resolved diffusive dynamic cross correlations of a pair of colloids in dense quasi-two-dimensional monolayers of identical particles are studied experimentally and theoretically at early times where motion is Fickian. In very dense systems where strong oscillatory equilibrium packing correlations are present, we find an exponential decay of the dynamic cross correlations on small and intermediate length scales. At large separations where structure becomes random, an apparent power law decay with an exponent of approximately −2.2 is observed. For a moderately dense suspension where local structural correlations are essentially absent, this same apparent power law decay is observed over all probed interparticle separations. A microscopic nonhydrodynamic theory is constructed for the dynamic cross correlations which is based on interparticle frictional effects and effective structural forces. Hydrodynamics enters only via setting the very short-time single-particle self-diffusion constant. No-adjustable-parameter quantitative predictions of the theory for the dynamic cross correlations are in good agreement with experiment over all length scales. The origin of the long-range apparent power law is the influence of the constraint of fixed interparticle separation on the amplitude of the mean square force exerted on the two tagged particles by the surrounding fluid. The theory is extended to study high-packing-fraction 3D hard sphere fluids. The same pattern of an oscillatory exponential form of the dynamic cross correlation function is predicted in the structural regime, but the long-range tail decays faster than in monolayers with an exponent of −3.

DOI: 10.1103/PhysRevE.92.052304 PACS number(s): 66.10.cg, 83.10.Pp, 05.20.Jj

I. INTRODUCTION

It was an enormous insight in the 19th century when Brownian motion was discovered in colloidal suspensions [1]. The implication that elementary units are persistently mobile is fundamental to our modern understanding of many material properties, particularly in soft matter [2]. To date, the space-time correlation of the Brownian motion of two particles can be used to extract the rheological properties of soft materials and biological media, an approach called two-point microrheology [3–6]. When dilute large tracer particles are suspended in a material, their long-range hydrodynamic interaction requires their Brownian motion to be correlated [7–11], and from its measurement the material mechanical properties can be deduced. Extensive effort has been given to understanding how an interface may change the correlation between the hydrodynamic diffusion of a pair of dilute tracer colloids [7,8].

For nondilute suspensions, the two-particle correlated motion cannot be a priori assumed to be solely controlled over all length and time scales by solvent-mediated hydrodynamic interactions. Multiple fundamental questions arise including the relative and absolute importance of (i) possible exponential suppression ("screening") [12–20] of hydrodynamic forces on "molecular" length scales, (ii) nonhydrodynamic two-particle dynamic correlations (which must exist) due to effective interparticle forces and fluid packing correlations [21–31], and (iii) fluid-density-dependent renormalization (modified prefactor, also called "screening" [15,16,32]) of the very long-range hydrodynamic interactions on scales where the fluid is a structural continuum. A high-level, poorly understood question is the relative importance of solvent-mediated hydrodynamic versus nonhydrodynamic mechanisms for inducing space-time displacement correlations in chemically and structurally distinct suspensions as a function of colloid density, length scale, and (effective) spatial dimensionality. This problem was recently studied theoretically for two large colloids suspended in unentangled and entangled polymer liquids [27].

In this article we employed integrated experimental and nonhydrodynamic statistical mechanical theory to study the correlated two-particle displacements of repulsive (charge-stabilized) colloidal suspensions that have sedimented to form an effectively two-dimensional fluid at a planar solid surface. Experimentally, the spatial dependence of dynamic displacement correlations is measured without using probes (tracers) over a wide range of length scales. Given the technical challenges associated with the measurements, we focus on the short-time regime for which (nearly) Fickian dynamics applies. Our experimental system has some similarities to that employed in recent studies of a single monolayer of a colloidal suspension tightly confined between two solid surfaces or at the interface between two bulk liquid phases [7–11]. However, our system is effectively a supported monolayer. This is potentially a major difference compared to prior studies from the point of view of the nature of hydrodynamic effects which are sensitive to boundary conditions in quasi-two-dimensional (quasi-2D) systems [11].

*sgranick@ibs.re.kr
†kschweiz@illinois.edu

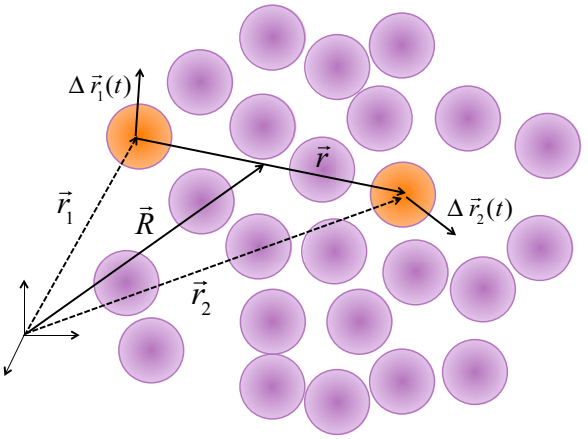

FIG. 1. (Color online) Coordinates used in our analysis. Two tagged spherical particles (orange) within a fluid of identical particles (purple) all of diameter σ are initially located at positions $\vec{r}_1$ and $\vec{r}_2$ in the laboratory frame. Alternatively, the center-of-mass, $\vec{R}$, and relative, $\vec{r}$, coordinates are defined. After a time t, the tagged particles are displaced by $\Delta\vec{r}_\alpha(t)$.

Figure 1 defines the relevant variables for our study. The two particles of interest are initially at positions $\vec{r}_\alpha$. After an elapsed time t, they displace by $\Delta\vec{r}_\alpha(t) \equiv \vec{r}_\alpha(t) - \vec{r}_\alpha$. Alternatively, their positions can be expressed in terms of center-of-mass (CM), $\vec{R}(t) \equiv [\vec{r}_1(t) + \vec{r}_2(t)]/2$, and relative, $\vec{r}(t) \equiv \vec{r}_2(t) - \vec{r}_1(t)$, coordinates. The dynamic displacement cross correlation tensor of the tagged particles is then defined as

$$\overleftrightarrow{C}_{12}(r_0,t) = \langle \Delta\vec{r}_1(t) \otimes \Delta\vec{r}_2(t)\rangle_{r_0}, \quad (1)$$

where $\otimes$ denotes a tensorial outer product, and the restricted ensemble average $\langle ...\rangle_{r_0}$ is performed at fixed interparticle separation r_0 at time t. For isotropic and homogeneous systems, $\overleftrightarrow{C}_{12}$ decays to zero at very large interparticle separations, and has only two independent elements: (i) the radial component along the separation vector, and (ii) the transverse component, defined as

$$C_{rr}(r_0,t) = \langle \Delta r_{1,r}(t)\Delta r_{2,r}(t)\rangle_{r_0}, \quad (2a)$$

$$C_{tt}(r_0,t) = \langle \Delta r_{1,t}(t)\Delta r_{2,t}(t)\rangle_{r_0}. \quad (2b)$$

Here, $\Delta r_{\alpha,r}(t) = \Delta\vec{r}_\alpha(t)\cdot\hat{r}_0$ is the displacement vector projected along the interparticle separation direction and $\Delta r_{\alpha,t}(t)$ is the projection onto one of the (equivalent) directions transverse to $\hat{r}_0$. The off-diagonal correlations between different directions vanish.

From a strictly hydrodynamic perspective, radial and transverse displacement correlations are expected to be comparable. On the other hand, when particles interact via a central pair potential of nonhydrodynamic origin, one expects radial correlations to dominate over transverse correlations. This is easy to see for two isolated particles since motion in any direction other than $\hat{r}_0$ is uncorrelated (no force). At finite particle densities, nonzero nonhydrodynamic transverse dynamic correlations will arise due to nonrandom packing, but the radial correlations are still expected to dominate. This expectation is confirmed in our experiments (see Sec. II), and for the remainder of this paper the focus is entirely on the radial correlations C_{rr} of Eq. (2a).

Experimentally, we find distinctive differences between the displacement correlations at moderate and high 2D packing fraction. The former shows, to a very good approximation, an apparent power law dependence of $C_{rr}(r_0)$ over all separations measured, while the latter exhibits exponential decaying correlations on the local structural scale which then cross over to the same apparent power law form at large interparticle separations. To understand our observations, we employ a first-principles, force-level, nonhydrodynamic statistical mechanical theory. Hydrodynamics enters only via the short-time single-particle diffusivity. Using experimental input for the required equilibrium pair correlation function $g(r)$, without any adjustable parameters the nonhydrodynamic theory agrees quantitatively with the measurements. The theory is then extended to make predictions for 3D hard sphere fluids for which experiments do not yet exist.

Section II describes our experimental approach and measurements of the single-particle mean square displacement (MSD). For context, a brief summary of relevant prior hydrodynamic theoretical work and experimental studies is presented in Sec. III, followed by the formulation of the general aspects of our nonhydrodynamic statistical mechanical approach for two-particle dynamics. Analytic results are derived for the displacement correlations in limiting regimes for quasi-2D fluids in Sec. IV. Section V presents our experimental results for displacement correlations, and quantitatively compares them to our theoretical predictions. The theory is applied to study 3D hard sphere fluids in Sec. VI. The paper concludes in Sec. VII with a brief discussion. Appendixes A and B provide technical theoretical details for the one- and two-particle problems, respectively.

II. EXPERIMENTAL APPROACH

Silica particles of diameter $\sigma = 2\ \mu$m (Shinshikyu, polydisperity index less than 0.001) were suspended in Milli-Q quality deionized water and stabilized by electrostatic repulsion. The solution was completely sealed between two glass cover slips (Gold Seal, thickness no. 1, 40 × 22 mm) with a spacer of height 120 μm. The particles naturally sedimented onto the bottom cover slip, forming a quasi-2D system where points of contact and centers of mass are coplanar; detailed analysis reveals extremely small vertical particle fluctuations. The particles were then observed under a bright field microscope. Two fluid area fractions are studied, $\eta_2 = 0.188$ and 0.503. At higher area fraction (0.584), the particles crystallize. We note that, in contrast to work by others on quasi-2D suspensions [8–11], our system has only one solid interface. This would seem to be an important difference with regard to the potential influence of hydrodynamic interactions on dynamic displacement correlations.

The positions of particles are tracked with a circle-finding algorithm in MATLAB and then linked into trajectories with unique particle IDs. Here, the potential dynamical uncertainty due to colloid motion can be neglected since the exposure time is much less than the time between frames. The static error due to inherent uncertainty in the tracking algorithm is on the order of 50 nm, roughly 3% of the particle diameter.

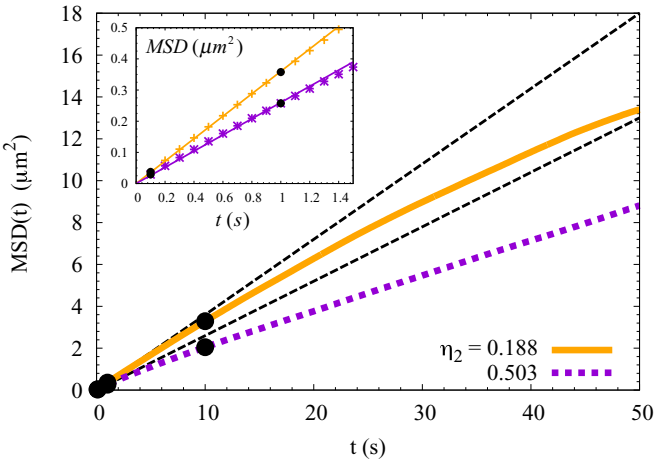

FIG. 2. (Color online) Experimental measurements of the single-particle mean square displacement (MSD) over long times up to 50 s (main frame) and over short times up to 1.5 s (inset). Results are shown for area fractions $\eta_2 = 0.188$ (orange curve, crosses in inset) and 0.503 (purple curve, stars in inset). The thin dashed black straight lines in the main frame (solid lines in inset) show fits to the Fickian form where the extracted self-diffusion constants are $D_{(1)} = 0.090\ \mu\text{m}^2/\text{s}$ and $0.065\ \mu\text{m}^2/\text{s}$ for the lower and higher area fractions, respectively. The black dots indicate the times at which the two-particle dynamic displacement correlations are measured.

To measure $g(r)$, the distances between all pairs of particles, $r_{\alpha\beta}$, were calculated from the experiments. The particle pairs were binned with an appropriate bin width (∼0.1 μm) and the distribution of all values of $r_{\alpha\beta}$ was divided by the kernel for a Poisson point process to eliminate edge effects [33]. Due to tracking errors and some unavoidable sample impurity, unphysical values can occur (separations smaller than the particle diameter). Pairs with such values of $r_{\alpha\beta}$ are a small minority and are eliminated in all subsequent analysis.

The measured dynamic displacements $\Delta\vec{r}_\alpha(t)$ from all the uniquely labeled trajectories are squared and averaged to calculate the single-particle mean square displacement $\text{MSD}(t) = \langle \Delta r_\alpha^2(t) \rangle$. By inspecting the MSD (Fig. 2) one sees that at short times the particles exhibit Fickian diffusion [2]:

$$\text{MSD}(t) = 4D_{(1)}t, \tag{3}$$

where Eq. (3) defines the quasi-2D single-particle diffusion constant $D_{(1)}$. At high liquid-like area fractions and long enough times, this changes as viscoelastic caging effects emerge. Regarding the relative diffusivity, we focus on short times, as shown by the black circles in Fig. 2. For area fraction $\eta_2 = 0.188$, the Fickian behavior holds at all three measurement times of C_{rr} and the self-diffusivity is $D_{(1)} = 0.090\ \mu\text{m}^2/\text{s}$. At $\eta_2 = 0.503$, Fickian motion with $D_{(1)} = 0.065\ \mu\text{m}^2/\text{s}$ roughly holds for all measurement times of C_{rr} except at $t = 10$ s when caging has begun.

For all particle pairs that can be tracked to an elapsed time t, we define two related quantities: (i) the average separation vector $\vec{r}_{\alpha\beta}(t) \equiv \frac{1}{2}\{\vec{r}_\beta(t) + \vec{r}_\beta\} - \frac{1}{2}\{\vec{r}_\alpha(t) + \vec{r}_\alpha\}$, and (ii) the product of projected displacements $\Delta r_{\alpha,\,r}(t)\Delta r_{\beta,\,r}(t)$. The pairs are first distributed among discrete bins according to $r_0 = |\vec{r}_{\alpha\beta}(t)|$ as in the calculation of $g(r)$; then all pairs within the bin centered at r_0 are averaged to give $C_{rr}(r_0,t) = \langle \Delta r_{1,\,r}(t)\Delta r_{2,\,r}(t) \rangle_{r_0}$. This allows us to directly access the dynamic correlations in dense suspensions without using invasive tracer particles. In general, $C_{rr}(r_0,t)$ decreases as separation and time lag grow, and the measurement becomes unreliable after roughly 2-3 decades of decay in amplitude. Bins are spaced logarithmically with most being wider than the particle diameter so that sufficient statistics can be collected. Hence, spatial features on the scale of the particle diameter and smaller in $C_{rr}(r_0,t)$ cannot be captured.

We find that the ratio of the transverse to the radial displacement correlation function, $C_{tt}(r_0,t)/C_{rr}(r_0,t)$ is typically small (<0.1), becoming increasingly so as the interparticle separation and time lag increase. Given our measurement noise level, this renders a reliable analysis of $C_{tt}(r_0,t)$ prohibitively difficult, and here we focus entirely on $C_{rr}(r_0,t)$. Finally, we note that unlike the conventional single-particle MSD measurements that depend only on time lag t, correlated diffusion has an extra spatial dependence and thus requires orders of magnitude more data to compute the averages presented in this article.

III. THEORY

We first briefly summarize recent hydrodynamic theory work and the corresponding experiments for colloid pair dynamics. A general nonhydrodynamic theory framework is then developed which is applicable to homogeneous fluids (no confining boundaries or interfaces) in any spatial dimension at short times.

A. Many-particle hydrodynamics and colloidal experiments

The classic hydrodynamics problem concerns the diffusive motion of one or two large particles (diameter σ) suspended in a small-molecule liquid [1–3]. For pair dynamics, the focus is generally on their correlated motion at large separations, $r_0 \gg \sigma$, where a continuum model is most appropriate. In dilute bulk 3D fluids, the displacement correlation function is very long range with a spatial dependence of [3]

$$\frac{C_{rr}(r_0,t)}{t} \propto \frac{1}{\eta_s r_0}, \quad r_0 \gg \sigma, \tag{4}$$

where at very short times (or in the dilute two-particle limit) η_s is the solvent viscosity, and at long times it is the low-frequency suspension viscosity.

Near an interface this behavior qualitatively changes. Combined experimental and theoretical work for two colloids (in the infinite-dilution limit) suspended at an elevation H above a solid surface found that in the (asymptotic) limiting regime $\sigma \ll H \ll r_0$ the displacement correlation decays much faster than in bulk 3D fluids, as [7]

$$\frac{C_{rr}(r_0,t)}{t} \propto r_0^{-3}, \quad \sigma \ll H \ll r_0 \tag{5}$$

Extensive studies [9–11] have been performed for quasi-2D dense suspensions (area fractions ranging from 0.254 to 0.547) composed of a single monolayer confined between two solid surfaces. At large interparticle separations, an apparently universal behavior for all packing fractions studied was

found [10]:

$$\frac{C_{rr}(r_0,t)}{t} \propto r_0^{-2}, \quad r_0 \gg \sigma \tag{6}$$

This power law decay is stronger than in 3D, but weaker than for the dilute problem near a single surface. On smaller length scales, oscillatory displacement correlations were measured that correlate with the equilibrium suspension structure [10]. A hydrodynamic theoretical analysis was performed that is in overall good agreement with the measurements, albeit with the introduction of two fit parameters to quantify amplitudes in the far and near field [10]. In this analysis, structural correlations *g(r)* enter only via their modification of the hydrodynamic mechanism for inducing displacement correlations. Specifically, the following additive form was derived [10]:

$$\frac{C_{rr}(r_0,t)}{t\,w^2} = \lambda\left(\frac{\sigma}{r_0}\right)^2 + C\eta_2\left(\frac{\sigma}{r_0}\right)^2 [g(r)-1], \tag{7}$$

where w is the film thickness, and C and λ are adjustable numerical prefactors. How the latter are influenced by suspension volume fraction and suspension viscosity is not a priori obvious. A surprising result is that the amplitude of the leading long-range contribution was measured to be (nearly) colloid concentration independent, and a hydrodynamics-based argument was advanced to explain this observation [10].

We note that the a priori validity of Eq. (7) at small interparticle separations is unclear given its continuum hydrodynamic basis. Moreover, the question of possible exponential screening of near-field hydrodynamic interactions [12–21] was not considered. Such exponential screening on "molecular" length scales due to multiple scattering effects is well established in 3D polymer solutions [14,15], and also for particle suspensions in rigid porous media [19,20]. However, it remains debated whether exponential screening exists in colloidal suspensions where all particles are mobile. Arguments for [12] and against [13,14] such screening have been advanced, as has the concept of partial screening [17], and also the idea that screening depends on nonuniversal features such as the range of electrostatic repulsions in colloidal fluids [18]. The issue of exponential screening in dense quasi-2D suspensions seems even more poorly understood. However, we emphasize that uncertainties about how to analyze hydrodynamics in quasi-2D suspensions are not relevant in a practical sense in this paper since we consider only a nonhydrodynamic mechanism for inducing dynamic displacement correlations. Of course, separating the consequences on correlated two-particle dynamics of hydrodynamic interactions and direct interparticle forces in dense suspensions is notoriously problematical. Moreover, for quasi-2D systems the relative importance is likely nonuniversal, given the sensitivity of hydrodynamic effects to sample configuration and hence boundary conditions [11]. We note that, as a matter of principle, the theory developed below could be unambiguously tested using Brownian dynamics simulations which remove many-particle hydrodynamic effects.

B. Nonhydrodynamic approach: Generalized Langevin equations

To analyze displacement cross correlations from a nonhydrodynamic perspective requires a statistical dynamical theory for the stochastic equations of motion of two tagged particles as a function of their separation in a dense fluid. Hydrodynamics will enter solely by employing the elementary single-particle Stokes-Einstein diffusivity to set the time scale for all further colloidal motion. The demonstrated agreement below between theory and experiment without fit parameters provides support for this starting point of our theoretical analysis.

The basis for the nonhydrodynamic theory is two coupled generalized Langevin equations (GLEs), which have been previously derived using Mori-Zwanzig methods for spherical particles [22–25,31]:

$$\zeta_0\frac{d\vec{r}_\alpha(t)}{dt} = -\frac{1}{\beta}\frac{\partial \ln g(\vec{r})}{\partial \vec{r}_\alpha} + \int_0^t d\tau \sum_{\gamma=1,2} K_{\alpha\gamma}(\vec{r},\, t-\tau)\frac{d\vec{r}_\gamma(\tau)}{d\tau} + \vec{\xi}_\alpha(t) + \vec{f}_\alpha^{\,Q}(t). \tag{8}$$

where $\beta = 1/k_BT$ is the inverse thermal energy, (α,γ) denote the tagged particle indices, Latin indices (i, j) are adopted to denote Cartesian components of vectors, and the interparticle separation is $\vec{r} \equiv \vec{r}_2 - \vec{r}_1$.

There are three main contributions in Eq. (8). (i) The drag force quantified by the very-short-time friction constant ζ_0, which is balanced by the random white noise force $\vec{\xi}_\alpha$. For colloidal suspensions, ζ_0 is the Stokes-Einstein value. (ii) The first term on the right-hand side of Eq. (8) involves the equilibrium potential of mean force (PMF), $W = -k_BT \ln g(\vec{r})$. It captures the reversible (nondissipative) component of interparticle forces due to the direct pair potential and the fluid-mediated component determined by nonrandom structural correlations. (iii) Viscoelastic effects associated with the space-time correlation of the forces exerted on the two tagged particles by the surrounding colloids enter via the nonlocal-in-time memory term $K_{\alpha\gamma}$. For appropriate time regime(s), it can be treated in a Markovian manner as a dissipative frictional drag force. The time autocorrelation of the slowly relaxing "random" $\vec{f}_\alpha^{\,Q}(t)$ is proportional to $K_{\alpha\beta}$ which depends on the instantaneous separation of the two tagged particles. From the fluctuation-dissipation theorem one has [31]

$$\langle \xi_{\alpha,i}(t)\xi_{\beta,j}\rangle = 2\,k_BT\;\delta(t)\,\delta_{\alpha\beta}\,\delta_{ij}\,\zeta_0, \tag{9a}$$

$$\left\langle f^Q_{\alpha,i}(t) f_{\beta,j}\right\rangle = \frac{k_BT}{d}\,\delta_{ij}K_{\alpha\beta}(t), \tag{9b}$$

where d is the spatial dimension, and the cross correlation between $\vec{\xi}$ and $\vec{f}$ vanishes.

Equation (8) can be simplified by transforming to center-of-mass and relative coordinates, yielding the (in general coupled) equations of motion:

$$\zeta_0\frac{d\vec{R}(t)}{dt} = \int_0^t d\tau\; K_R(\vec{r}, t-\tau)\frac{d\vec{R}(\tau)}{d\tau} + \vec{\Xi}(t) + \vec{F}^{\,Q}(t), \tag{10a}$$

$$\zeta_0\frac{d\vec{r}(t)}{dt} = -\frac{1}{\beta}\frac{\partial \ln g[2r(t)+r_0]}{\partial r} + \int_0^t d\tau\; K_r(\vec{r},\, t-\tau)\frac{d\vec{r}(\tau)}{d\tau} + \vec{\xi}(t) + \vec{f}^{\,Q}(t), \tag{10b}$$

where $K_R = K_{11} + K_{12}$ and $K_r = K_{11} - K_{12}$ are the CM and relative memory functions, respectively. Additionally, $\vec{\Xi} \equiv (\vec{\xi}_1 + \vec{\xi}_2)/2$ and $\vec{\xi} \equiv \vec{\xi}_2 - \vec{\xi}_1$ denote the corresponding white noise random forces for the center of mass and relative variables, while $\vec{F}$ and $\vec{f}$ denote the slowly relaxing random forces with analogous definitions in terms of $\vec{f}_1$ and $\vec{f}_2$. The cross correlations of Eq. (2) can then be written as

$$\langle \Delta r_{1,r}(t)\, \Delta r_{2,r}(t) \rangle_{r_0} = \langle \Delta R_r(t)\, \Delta R_r(t) \rangle_{r_0} - \tfrac{1}{4} \langle \Delta r_r(t)\, \Delta r_r(t) \rangle_{r_0}. \tag{11}$$

Statistical mechanical approximations are necessary to compute the memory functions and thus solve Eqs. (8)–(11) for the single-particle and relative dynamic correlations.

C. Two-particle mode coupling theory

To calculate the memory function we employ a simple mode coupling theory (MCT) [25–31] that has been successfully utilized for different problems recently [25–27] but the derivation of which has only been sketched. The latter is now given in Appendix B and is summarized below.

Assuming that the relevant slow dynamical variable involves only density fluctuations, the force on a tagged particle is projected onto the slow bilinear density modes, which in Fourier space are $\rho_\alpha(k)\rho_c(-k)$. Here, $\rho_\alpha(\vec{k}) = e^{-i\vec{k}\cdot\vec{r}_\alpha}$ is the Fourier transform of the single-particle density associated with either tagged particle, and $\rho_c(k)$ is the Fourier-transformed collective density of the surrounding particles. Unlike single-particle (naïve) MCT (see Appendix A), here a matrix projection is employed since two particles are of interest. A standard Gaussian factorization of four point correlations into a product of two point functions is employed to close the theory. Detailed analysis (see Appendix B) yields the center of mass (R,+) and relative (r,−) memory functions:

$$K_{R,r}(t) = \frac{\rho_d}{\beta\, d} \int \frac{d^d\vec{k}}{(2\pi)^d}\, \frac{k^2 h^2(k)}{S(k)}\, \frac{1}{1 \pm \omega_{12}^{(d)}(k)}\, \Gamma_s(k,t)\, \Gamma_c(k,t), \tag{12}$$

where the + (−) sign applies for R (r). In Eq. (12), $h(k)$ is the nonrandom pair distribution function in Fourier space, $S(k) = 1 + \rho_d\, h(k)$ is the static structure factor, and Γ_s (Γ_c) is the single-particle (collective) dynamic density-density correlation function normalized to unity at $t = 0$. The quantity $\omega_{12}^{(d)}(k)$ captures the constraint on the two tagged particles that their separation in space is fixed when determining the displacement correlation function.

To make further progress we invoke two simplifications motivated by the specific experimental conditions of interest: (i) the tagged particles are effectively at a fixed separation during the measurement of cross correlation, and (ii) only short-time dynamics is investigated such that many-body caging and non-Markovian effects are absent. These simplifications have several consequences. First, the fixed separation ensemble is invoked to calculate the constraint function $\omega_{12}^{(d)} = \langle e^{-i\vec{k}\cdot(\vec{r}_2 - \vec{r}_1)} \rangle_{r_0}$, which is averaged over the solid angle in the proper dimension d. An elementary calculation yields

$$\omega_{12}^{(2)}(k) = J_0(kr_0), \tag{13a}$$

$$\omega_{12}^{(3)}(k) = j_0(kr_0) = \sin(kr_0)/kr_0, \tag{13b}$$

where J_0 is the cylindrical Bessel function, and j_0 is the spherical Bessel function. Conditions (i) and (ii) also have implications for computing the dynamical density-density correlation functions (or propagators) $\Gamma_\alpha(k,t)$. The fixed separation constraint implies that dynamical decorrelation of the forces on the two-tagged particles is solely due to relaxation of the surrounding fluid; hence we set $\Gamma_s \approx 1$. A standard short-time diffusive form of the collective dynamic density-density fluctuation structure factor Γ_c is adopted, since the measurements are taken before the onset of viscoelastic effects (Fig. 2). Thus, in a time regime where displacements are Fickian one has [2,34,35]

$$\Gamma_c(k,t) = \exp\left[-\frac{k^2 D_0 t}{S(k)} \right], \tag{14}$$

where $D_0 = k_B T/\zeta_0$ is the single-particle short-time diffusion constant.

Since the particles are effectively fixed during the measurement of $C_{rr}(r_0)$, the potential of mean force is a constant and can be dropped in Eq. (10). Adopting the Fickian assumption in Eq. (10) allows us to define the renormalized center-of-mass friction constant $\zeta_{rr}^{(R)} \equiv \zeta_0 + \int_0^\infty dt\; K_R(t)$. The center-of-mass correlations are then given by $\langle [\Delta R_r(t)]^2 \rangle_{r_0} = t(k_B T/\zeta_{rr}^{(R)})$, and similarly for the relative coordinate. Using these solutions of Eq. (10) in Eq. (11) yields

$$D_{rr}^{\text{non-HD}} = k_B T \left(\frac{1}{\zeta_{rr}^{(R)}} - \frac{1}{\zeta_{rr}^{(r)}} \right), \tag{15}$$

where $D_{rr}^{\text{non-HD}}(r_0)$ is the separation-dependent nonhydrodynamic relative diffusion constant $\langle \Delta r_{1,r}(t)\, \Delta r_{2,r}(t) \rangle_{r_0} \equiv D_{rr}^{\text{non-HD}}(r_0)\, t$. Note that the cross correlations must be smaller than their diagonal analog $\langle \Delta\vec{r}_1(t) \cdot \Delta\vec{r}_2(t) \rangle \leqslant \langle \Delta r_1^2(t) \rangle$, which implies the rigorous bound $D_{rr}^{\text{non-HD}} \leqslant 4D_{(1)}$.

Combining Eqs. (12) and (10) with the definition of the friction constants above Eq. (15), and performing the time integral, yields

$$\frac{\zeta_{rr}^{(R)}}{\zeta_0} = 1 + \frac{\rho_d}{d} \int \frac{d^d\vec{k}}{(2\pi)^d}\, \frac{h^2(k\sigma)}{1 \pm \omega_{12}^{(d)}(kr_0)}. \tag{16}$$

Equations (13), (15), and (16) form the foundation of the nonhydrodynamic theory. It is a general starting point to analyze the short-time dynamic displacement correlations of quasi-2D or 3D systems of spherical particles interacting through arbitrary pair potentials at any fluid density in the absence of many-particle hydrodynamics. Note that our treatment of dynamic displacement correlations in quasi-2D systems is not sensitive to system boundary conditions, in contrast to the hydrodynamics-mediated mechanism.

IV. THEORY IMPLEMENTATION AND ANALYTIC RESULTS FOR QUASI-2D SUSPENSIONS

A. Model for structural input

To implement the dynamical theory requires the equilibrium pair structure. While two-dimensional integral equation theory for hard disks could potentially be employed [2], this likely is not quantitatively appropriate for our experimental colloidal suspension which is neither literally 2D nor literally a hard core system. We instead utilize the measured equilibrium pair correlation function shown in Fig. 3 for two area fractions $\eta_2 = \rho_2 \pi \sigma^2/4$ of 0.188 and 0.503. The solid curves are the experimental results and the dotted curves are analytic fits to them. For $\eta_2 = 0.503$, the following model is employed:

$$g(r) = \begin{cases} 0, & r < \sigma, \\ 1 + (Ae^{-8(r-\sigma)/\lambda} + Be^{-(r-\sigma)/\xi_{\rm struc}}) \sin\left[\frac{2\pi}{\lambda}(r-\sigma)\right], & r \geqslant \sigma. \end{cases} \tag{17}$$

Equation (17) has four parts: (i) a hard core constraint where $g(r) = 0$, (ii) oscillations with a wavelength on the order of the particle size, $\lambda = 1.1\,\sigma$, (iii) an exponential envelope with decay length $\xi_{\rm struc} = 2.05\,\sigma$ and amplitude $B = 1$, and (iv) another exponential with amplitude $A = 9$ and a shorter decay length to capture the contact peak region. For $\eta_2 = 0.188$, no distinct oscillations exist in the experimental distribution function, and Eq. (17) is not appropriate. Instead we model $g(r)$ as a piecewise continuous function: for $r < \sigma$ a hard core is employed, for $\sigma \leqslant r \leqslant 2.0\,\sigma$ an interpolation form is used, and for $r > 2.0\sigma$ the structure is taken to be random, i.e., $g(r) = 1$. Figure 3 shows that the two analytic models capture reasonably well the measured pair correlation functions.

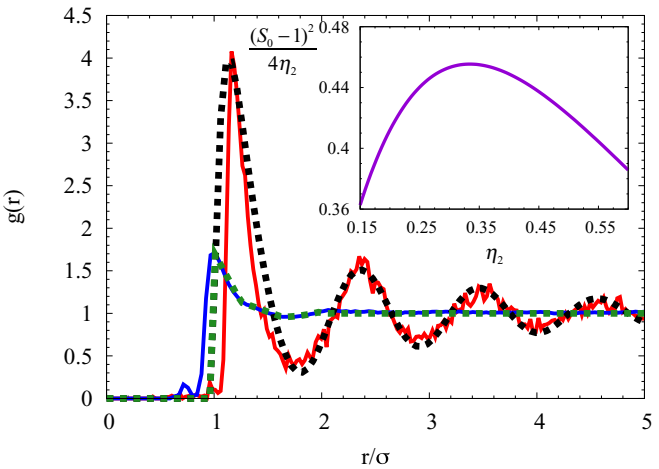

FIG. 3. (Color online) Pair correlation functions $g(r)$, where the separation distance r is scaled by the colloid diameter, are plotted against the normalized separation. Smoothed experimental results (solid curves) are shown for two area fractions $\eta_2 = 0.188$ (lower magnitude, blue) and $\eta_2 = 0.503$ (higher magnitude, red). The dotted curves are the analytic model results discussed in Sec. IV A. Inset: The prefactor of the long range correlation tail evaluated for 2D hard disks [Eq. (22)], plotted as a function of area fraction η_2, is nearly constant over the measured range of area fraction.

B. Analytic limits

Before presenting a full numerical treatment of the relative diffusion, three analytic limits are investigated: (i) zero separation $r_0 \to 0$, (ii) large separations $r_0 \gg \sigma$, and (iii) intermediate separations $r_0 \approx \sigma + \xi_{\rm struc}$.

The first limit is easily taken since the constraint function for zero separation is $\omega_{12}(0) = 1$. Using this in Eq. (16), the CM friction becomes equal to the single-particle friction $\zeta^{(R)} = \zeta_{(1)}$ (see Appendix A), and the relative friction diverges, $\zeta^{(r)} \to \infty$. From Eq. (15), this implies that the cross-correlation reduces to the single particle diffusivity $D_{rr} \to D_{(1)}$. Since the cross correlations decay with interparticle separation, the necessary physical limit that $D_{rr} \leqslant 4D_{(1)}$ is guaranteed to hold.

To work out the limits (ii) and (iii), it is instructive to first nondimensionalize the integral in Eq. (16) using $\vec{q} = \vec{k} r_0$. Performing the solid angle integral then yields

$$\frac{\zeta_{rr}^{(R)}}{\zeta_0^{(r)}} = 1 + \frac{4\eta_d(d-1)}{(2\pi)^d}\left(\frac{\sigma}{r_0}\right)^d \int_0^\infty dq\, q^{d-1} \frac{\tilde{h}^2(q\sigma/r_0)}{1 \pm \omega_{12}(q)}, \tag{18}$$

where $\eta_d = \rho_d \pi \sigma^d/2d$ is the d-dimensional packing fraction, and $\tilde{h}(k) = h(k)/\sigma^d$. Now the limits can be explicitly taken. For the $r_0 \gg \sigma$ large separation limit, the integral in Eq. (18) is dominated by its $q \to 0$, long wavelength limit. To leading order, the equilibrium pair structure in Fourier space is constant, $\tilde{h}(q\sigma/r_0) \approx \tilde{h}(0) = \pi(S(0)-1)/4\eta_2$, where $S(0) \equiv S(q=0)$ is the dimensionless isothermal compressibility [2]. Also in this limit, the dominant contribution to the dynamic cross correlations is due to $\omega_{12}^{(2)}(q) \approx 1 - q^2/4 + \vartheta(q^4)$. For the center of mass and relative frictions one thus finds

$$\frac{\zeta_{rr}^{(R)}}{\zeta_0} = 1 + \frac{\eta_2}{\pi^2}\left(\frac{\sigma}{r_0}\right)^2 \tilde{h}^2(0) \int_0^1 dq\, \frac{q}{2}, \tag{19a}$$

$$\frac{\zeta_{rr}^{(r)}}{\zeta_0} = 1 + \frac{\eta_2}{\pi^2}\left(\frac{\sigma}{r_0}\right)^2 \tilde{h}^2(0) \int_0^1 dq\, \frac{4}{q}. \tag{19b}$$

In Eq. (19) the upper limit of the integrals has been replaced by unity to be consistent with the small wave vector expansion. The CM integral is easily evaluated. For the relative coordinate friction, in 2D a low wave vector cutoff $r_0 \leqslant r_{\rm max}$ is necessary for convergence and reflects the finite system size. Performing the integrals yields

$$\frac{\zeta_{rr}^{(R)}}{\zeta_0} \approx 1 + \frac{\eta_2}{4\pi^2}\left(\frac{\sigma}{r_0}\right)^2 \tilde{h}^2(0), \tag{20a}$$

$$\frac{\zeta_{rr}^{(r)}}{\zeta_0} \approx 1 + \frac{4\eta_2}{\pi^2}\tilde{h}^2(0)\left(\frac{\sigma}{r_0}\right)^2 \ln\left(\frac{r_{\rm max}}{r_0}\right). \tag{20b}$$

The logarithmic factor in Eq. (20b) is a "marginal" feature in the sense that it is peculiar to 2D, vanishing in higher dimensionality.

Combining the friction constants in Eq. (20) with Eq. (15) leads to a long distance nonhydrodynamic cross correlation that to leading order in σ/r_0 is

$$D_{rr}^{\rm non-HD} \approx D_0 \frac{4\eta_2}{\pi^2}\tilde{h}^2(0)\left(\frac{\sigma}{r_0}\right)^2 \left[\ln\left(\frac{r_{\rm max}}{r_0}\right) - \frac{1}{16}\right], \tag{21}$$

which is valid if $r_0 \ll r_{\max}$. Note the slowly decaying power law contribution with an exponent of -2. Interestingly, this is the same power law form derived from a hydrodynamic analysis for quasi-2D systems confined by two solid surfaces [9,10]. However, it is important to emphasize that the prefactor in Eq. (7) differs from its hydrodynamic analog [10]. The logarithmic factor in Eqs. (20b) and (21) arises simply from dimensional analysis in conjunction with the small wave vector limit of the constraint which without loss of generality is $\omega_{12} \approx 1 + Bq^2$. Physically, the constraint modifies the amplitude of fluid-mediated force correlations between the two particles as a function of their separation. The logarithmic contribution reduces, not enhances, the friction with increasing r_0.

Quantitative implementation of the theory requires a value for $r_{\max}$. The experimental system is a circular cell with radius $R = 1.5$ cm; hence the cutoff is roughly $r_{\max}/\sigma \approx 7500$. For the experimentally relevant regime of $\sigma \ll r_0 \ll r_{\max}$, numerical calculations reveal that Eq. (21) reduces roughly to an apparent power law with the form

$$\frac{D_{rr}^{\text{non-HD}}}{D_0} \approx \frac{[S(0)-1]^2}{4\eta_2}\, r_0^{-2.2}. \tag{22}$$

This apparent scaling form depends on neither fluid structure nor area fraction. However, its magnitude (amplitude) does depend on the area fraction both directly and indirectly via the dimensionless isothermal compressibility, $S(0)$. One can gain intuition concerning this variation from the 2D hard disk equation of state [36]. The amplitude is plotted in the inset of Fig. 3 for area fractions relevant to experiments, $0.15 \leqslant \eta_2 \leqslant 0.6$. One sees a weak nonmonotonic variation of only $\sim\pm 10\%$. Such a variation very likely is in the noise of experimental measurement of the long range tail of the displacement correlation function.

The final (intermediate) regime is when interparticle separations are beyond the (short) density correlation length, $r_0 \gtrsim \sigma + \xi_{\text{struc}}$, but structural correlations are still relevant. Here, Eq. (18) is dominated by the large wave-vector limit, $q \to \infty$, and $\omega_{12}(q)$ is small. Hence the integrals can be Taylor expanded to give

$$\frac{\zeta_{rr}^{(R)(r)}}{\zeta_0} \approx 1 + \frac{\eta_2}{\pi^2}\left(\frac{\sigma}{r_0}\right)^2 \int_0^\infty dq\, q\tilde{h}^2(q\sigma/r_0)[1 \mp \omega_{12}(q)]. \tag{23}$$

If $\omega_{12}(q) \equiv 0$, Eq. (23) reduces to the single-particle friction constant (see Appendix A):

$$\zeta_{(1)}/\zeta_0 = 1 + \left(\eta_2\sigma^2/\pi^2 r_0^2\right)\int_0^\infty dq\, q\tilde{h}^2(q\sigma/r_0). \tag{24}$$

The final contribution associated with $\omega_{12} \neq 0$ is the two-particle correction to the cross correlation:

$$\delta\zeta_{rr}/\zeta_0 = \eta_2\sigma^2/\pi^2 r_0^2 \int_0^\infty dq\, q\tilde{h}^2(q\sigma/r_0)\omega_{12}(q). \tag{25}$$

Using these definitions, the CM friction can be written as $\zeta_{rr}^R \approx \zeta_{(1)} - \delta\zeta_{rr}$, and the relative friction as $\zeta_{rr}^r = \zeta_{(1)} + \delta\zeta_{rr}$. Substitution into Eq. (15) and algebraic simplification yields

$$D_{rr}^{\text{non-HD}} \approx D_0 \frac{2\delta\zeta_{rr}/\zeta_0}{(\zeta_{(1)}/\zeta_0)^2 - (\delta\zeta_{rr}/\zeta_0)^2}. \tag{26}$$

To first order in the small quantity $\delta\zeta_{rr}/\delta\zeta_0$ one obtains

$$D_{rr}^{\text{non-HD}} \approx \left(2D_{(1)}^2/D_0\right)(\delta\zeta_{rr}/\zeta_0). \tag{27}$$

We note that the structural correlations always enter as the square of $h(q)$ in the above analysis, in qualitative contrast to the hydrodynamic result of Eq. (7). The reason is that the friction constant renormalization arises from force-force time correlations, not structural modification of solvent-mediated hydrodynamic interactions.

To proceed requires a structural model. To maintain analyticity, the expression in Eq. (17) is simplified by ignoring the hard core constraint and oscillations, thereby yielding $g(r) \approx 1 + Be^{-(r-\sigma)/\xi}$. We show in the next section that the results derived using this simplification are consistent with our full numerical calculations. Performing the 2D Fourier transform $h(k) = -2\pi \int_0^\infty dr\, rh(r)J_0(kr)$ leads to the wave vector space structure

$$h(k) = -2\pi\, Be^{\sigma/\xi}\frac{\xi^2}{(1+k^2\xi^2)^{3/2}}. \tag{28}$$

Using Eq. (28) in Eq. (26), the resulting integral for $\delta\zeta_{rr}$ can be analytically evaluated, yielding a relative correlation

$$D_{rr}^{\text{non-HD}} = \frac{D_{(1)}^2}{D_0}\, B^2\eta_2\, e^{2\sigma/\xi}\, \frac{r_0^2}{\sigma^2} K_2(r_0/\xi), \tag{29}$$

where $K_2(x)$ is the modified Bessel function. For separations larger than the decay length $r \gtrsim \xi_{\text{struc}}$, Eq. (29) scales roughly as an exponential:

$$\frac{D_{rr}^{\text{non-HD}}}{D_0} \sim \left(\frac{D_{(1)}}{D_0}\right)^2 \left(\frac{\sigma}{\xi}\right)^2 \eta_2 e^{2\sigma/\xi} e^{-r_0/\xi} \tag{30}$$

Based on the numerical calculations presented in the next section, we find that the analytic form in Eq. (30) holds for separations $\xi_{\text{struc}} \lesssim r_0 \lesssim 8\xi_{\text{struc}}$. It will increasingly dominate the full numerical result at higher area fractions where the structural (density correlation) decay length is larger. Additionally, since the hard core constraint and the oscillations of $g(r)$ have been ignored in deriving Eq. (30), the result applies only to the envelope of the numerical results. Curiously, the exponential form of Eq. (30) with a dynamic decay length equal to the structural correlation length agrees with the hydrodynamic result in Eq. (7). This would seem to be another accidental correspondence between the hydrodynamic and nonhydrodynamic mechanisms for quasi-2D systems.

V. EXPERIMENTAL RESULTS AND COMPARISON TO THEORY

We now apply the theory to make no-adjustable-parameter predictions for the displacement correlations in quasi-2D and quantitatively compare them to our experimental data. To do so, $h(k)$ is numerically obtained from the models in Sec. IV A. Inserting this $h(k)$ and the constraint condition of Eq. (13a) into Eq. (16), and performing the integral numerically, yields the CM and relative friction constants. From this, D_{rr} follows from Eq. (15). These numerical results differ (as a matter of principle) from the analytic results in Sec. IV B, the derivation of which depended on technical simplifications.

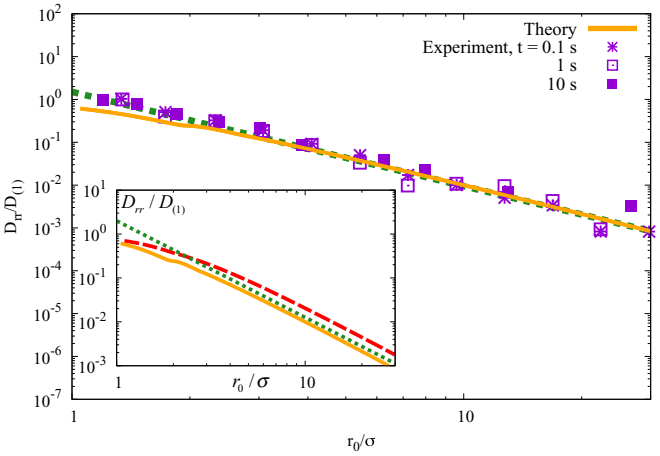

FIG. 4. (Color online) For the lower area fraction $\eta_2 = 0.188$ sample, the 2D dynamic cross correlations, normalized by the single-particle diffusivity, are plotted on log-log scales as a function of normalized particle initial separation. The experiments (points) concern various short times at which single-particle diffusion is (nearly) Fickian, $t = 0.1, 1, 10$ s; the corresponding no-adjustable-parameter theoretical predictions are shown as the solid curve. As a guide to the eye, the dotted green line with slope -2.2 is also shown. Inset: Same as the main frame. The full numerical theoretical result (solid curve) and power law scaling (dotted line) are compared to a simplified calculation that assumes the structure is random beyond the particle diameter (dashed line).

Figures 4 and 5 show the experimental data and numerical theoretical results for packing fractions $\eta_2 = 0.188$ and $\eta_2 = 0.503$, respectively. The data (points) and theoretical results (curves) for the cross diffusivity $D_{rr} = C_{rr}(t)/t$, normalized by the single-particle diffusivity, $D_{(1)}$, are plotted as a function of the tagged particles' separation r_0. In the theory, the cross

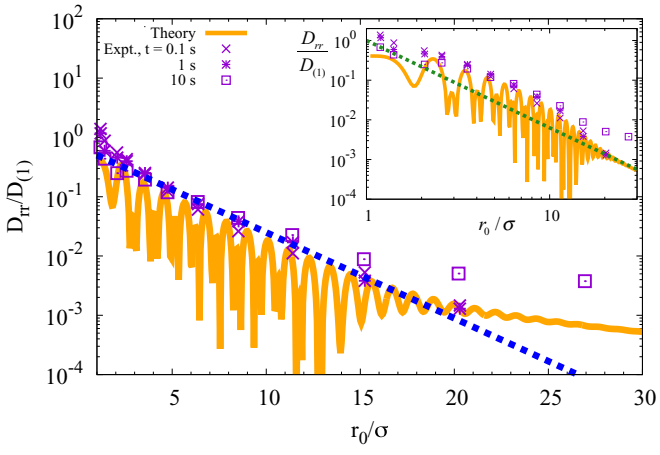

FIG. 5. (Color online) 2D dynamic cross correlations (normalized by the single-particle diffusivity) for the higher area fraction $\eta_2 = 0.503$ sample are plotted on semilogarithmic scales as a function of normalized particle separation. The dotted blue line is an exponential fit to the amplitude of the theoretical curve with decay length $\xi_{rr} = 3.0\sigma$. Inset: Log-log plot of the same results as in the main frame. The dotted line with slope -2.2 expresses the power law $D_{rr} \sim r_0^{-2.2}$.

diffusivity changes sign due to the oscillations associated with the pair structure; we plot its absolute value $|D_{rr}|$. Note that the experimental data at different times collapse quite well for both area fractions, with the exception of data for $\eta_2 = 0.503$ at the longest time of $t = 10$ s. The former behavior provides experimental support for the Fickian renormalized friction idea employed in the theory at the area fractions and time scales explored experimentally.

For $\eta_2 = 0.188$, the main frame in Fig. 4 shows the correlations in a log-log representation. Within experimental uncertainty, the observed correlations decay as a power law as $D_{rr} \sim r_0^{-2.2}$ (dotted line) over the entire range of separations studied (up to 40 microns). The theoretical calculation (solid line) follows an essentially identical apparent power law scaling as expected from the analytic analysis in Sec. IV B. The latter suggests this scaling should hold only for separations beyond the range of the structural correlations. However, at this low area fraction the structural correlations are very weak (Fig. 3). The theory and experiment quantitatively agree without adjustable parameters.

The inset of Fig. 4 shows theoretical results for the low area fraction system compared to an even simpler calculation which assumes a literal random structure outside the hard core diameter [$g(r \geqslant \sigma) = 1$] (red dashed line). The close agreement buttresses our conclusion that short range oscillatory structural correlations are of nearly negligible importance, and further justifies the power law scaling [Eq. (22)] over all measured separations. However, recall that hard core interparticle repulsions do set the amplitude of our effective power law prediction in Eq. (22) via the dimensionless compressibility or long wavelength density fluctuation amplitude, S(0).

Figure 5 shows results for the high area fraction system. One sees two distinct regimes of behavior in the dynamic cross correlations. At small and intermediate separations ($\sigma \lesssim r_0 \lesssim 15\sigma \approx 8\xi_{\text{struc}}$), the cross correlation decays roughly exponentially $D_{rr} \sim \mathrm{e}^{-r/\xi_{rr}}$ (main, blue dashed curve). For the experimental data, $\xi_{rr} = (3.0 \pm 0.1)\sigma$, close to the structural decay length $\xi_{\text{struc}} = 2.05\,\sigma$. For large separations where structural correlations randomize, the scaling becomes a power law (inset) as for the lower area fraction suspension and with the same apparent exponent. This limit is somewhat difficult to see in the experimental data because of the increased statistical uncertainty at large separations. But within this uncertainty, the tail amplitude for the two experimental samples is essentially identical, consistent with the nonhydrodynamic theory as discussed below Eq. (22). Thus, the two regimes observed in the correlated displacement function data agree with the analytic theoretical analysis. We do note that at the longest time of $t = 10$ s the D_{rr} data do not collapse at large separations, likely as a consequence of the onset of caging effects as discussed previously (Fig. 2).

The solid curves in Fig. 5 show the full numerical predictions, and there is good agreement with the experimental results with the caveat that caging is observed at $t = 10$ s. For $\sigma \lesssim r_0 \lesssim 18\sigma$, exponential decay is seen, while for $r_0 \gtrsim 18\sigma$ the same power law behavior is seen as found at the lower area fraction, and with similar amplitude. In the small separation exponential regime, the theoretical results exhibit the expected oscillations with a wavelength of order the particle diameter due to short-range packing correlations. The experiments

exhibit little or no evidence of oscillations, mainly, we suspect, owing to the discrete data binning. This leads to an averaging over the oscillations and the measurements determine only the envelope of the dynamic correlations. The available statistical data set does not allow us to reliably parse the data into smaller bin sizes. Focusing on the envelope, one concludes that the theory is consistent with experiment.

Finally, note the nonsystematic locations and amplitudes of apparent minima of the theoretical results in Fig. 5. These arise from the predicted oscillatory form of $D_{rr}(r_0)$. Since only the magnitude of D_{rr} is plotted, these minima indicate sign changes due to the effect of oscillatory packing correlations on pair diffusion. We assign no practical importance or physical interpretation to the precise magnitudes of these low amplitude features, especially given their inevitable sensitivity to the discrete nature of the numerical calculations performed to construct the curves.

VI. THEORETICAL PREDICTIONS FOR 3D HARD SPHERE FLUIDS

We are not aware of any experiments on 3D dynamic cross correlations in colloidal suspensions; indeed, to obtain such data would be a formidable technical challenge. But the theory is easily applied in 3D to make predictions that are hopefully testable in the future by experiment and/or simulation. Here we consider suspensions and (overdamped) one-component fluids in the absence of long-range hydrodynamic interactions. Unlike the analysis of the 2D suspension, experimental data for the required $g(r)$ over a wide range of volume fractions $\eta_3 = \rho_3 \pi \sigma^3/6$ is not readily available. We consider the hard sphere fluid, and employ the Ornstein-Zernike equation with Percus-Yevick closure [2] to compute $h(k)$.

A. Analytic limits

We first consider the two analytic limits. For large separations $r_0 \gg \sigma$, Eq. (18) can be analyzed in the small wave vector limit in an analogous manner to what was done in Sec. IV B. In 3D, one has $\omega_{12}^{(3)}(q) \approx 1 - q^2/6 + \vartheta(q^4)$ and the equilibrium structure in Fourier space, $h(q)$, is taken to be its $q = 0$ limit value. The friction constants follow as

$$\frac{\zeta_{rr}^{(R)}}{\zeta_0} = 1 + \frac{\eta_3}{\pi^3}\left(\frac{\sigma}{r_0}\right)^3 \tilde{h}^2(0) \int_0^1 dq\, \frac{q^2}{2}, \tag{31a}$$

$$\frac{\zeta_{rr}^{(r)}}{\zeta_0} = 1 + \frac{6\eta_3}{\pi^3}\left(\frac{\sigma}{r_0}\right)^3 \tilde{h}^2(0) \int_0^1 dq\,. \tag{31b}$$

In contrast to the 2D case, there is no logarithmic correction in 3D. Performing the integrals in Eq. (31), the dynamic cross correlation function is

$$\frac{D_{rr}^{\text{non-HD}}}{D_0} = \frac{11}{2\pi^3}\frac{[S(0)-1]^2}{\eta_3}\left(\frac{\sigma}{r_0}\right)^3 \tag{32}$$

Thus, in the large separation limit the nonhydrodynamic correlations scale as a power law with exponent of -3, corresponding to a faster decay than in quasi-2D. But similarly to the latter, their amplitudes depend on the fluid dimensionless isothermal compressibility and packing fraction.

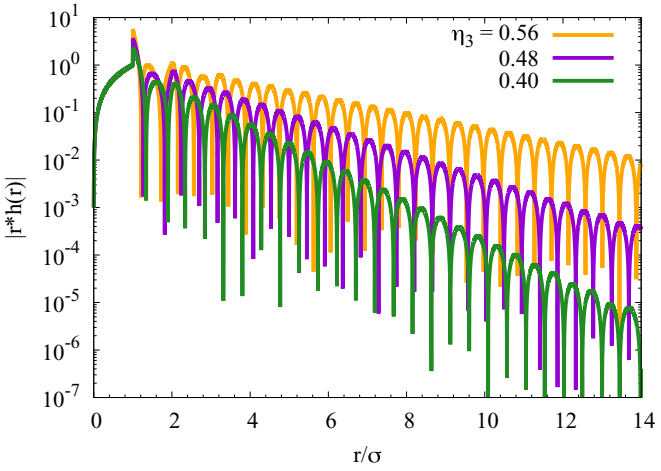

FIG. 6. (Color online) The magnitude of the nonrandom part of the pair distribution function of the 3D hard sphere fluid multiplied by the dimensionless interparticle separation $|rh(r)|$, plotted logarithmically against the dimensionless interparticle separation for packing fractions $\eta_3 = 0.56,\ 0.48,\ 0.40$ from top to bottom. The maxima obey a Yukawa decay as expected.

For intermediate separations, analysis analogous to Sec. IV B. is performed by taking the $q \to \infty$ limit. The friction integrals in Eq. (18) are again expanded for small ω_{12}. With the 3D equivalents for $\zeta_{(1)}$ and $\delta\zeta_{rr}$, Eq. (26) remains unchanged and the first order correction integral must be calculated. In 3D, the pair distribution function exhibits the usual oscillations and outside of the correlation length ($r > \xi_{\text{struc}}$) has a Yukawa envelope $h(r) \approx B\sigma e^{-r/\xi_{\text{struc}}}/r$, as seen in Fig. 6. The structural correlation length monotonically grows from $\xi_{\text{struc}} = 1.1\ \sigma$ for $\eta_3 = 0.40$, to $2.7\ \sigma$ for $\eta_3 = 0.56$.

Performing the 3D Fourier transform of the above $h(r)$ yields

$$h(k) = \frac{4\pi\ B\sigma {\xi_{\text{struc}}}^2}{1 + k^2 {\xi_{\text{struc}}}^2}. \tag{33}$$

The resulting integral for $\delta\zeta_{rr}$ can be analytically evaluated, yielding

$$D_{rr}^{\text{non-HD}} = \frac{D_{(1)}^2}{D_0}\, 8\, B^2\, \eta_3 \frac{\xi_{\text{struc}}}{\sigma} e^{-r_0/\xi_{\text{struc}}}. \tag{34}$$

Thus, the nonhydrodynamic cross correlations again scale exponentially with separation at intermediate interparticle separations $D_{rr}^{\text{non-HD}} \propto e^{-r_0/\xi_{\text{struc}}}$. It is interesting, and somewhat surprising, that both the (quasi-)2D and 3D dynamic correlations for hard repulsive particles at intermediate separations have exponential envelopes.

B. Model calculations

Numerical analysis of the 3D dynamic cross correlations was performed for many fluid packing fractions; here we show representative dense fluid results for $\eta_3 = 0.40,\ 0.48,\ 0.56$, where the last value is in the "glassy dynamics" regime.

Figure 7 shows calculations in log-linear (main) and log-log formats (inset). As predicted by the analytic analysis, there are two regimes of behavior. At intermediate separations, the

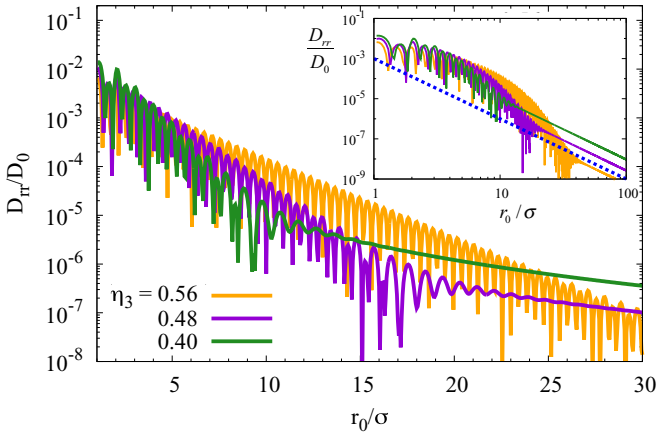

FIG. 7. (Color online) Predicted dynamic cross correlations in dense 3D hard sphere fluids, normalized by the single-particle bare diffusivity, are plotted semilogarithmically as a function of the normalized separation of the two tagged particles. Results are shown for packing fractions $\eta_3 = 0.56,\ 0.48,\ 0.40$ (top to bottom at intermediate separations). Inset: Same as main frame but in a log-log format. The dotted line shows the power law $D_{rr} \sim r_0^{-3}$.

displacement correlations exhibit particle diameter scale oscillations with an exponential envelope. Within the numerical uncertainty, there is complete agreement between the dynamic decay length ξ_{rr} and its structural analog ξ_{struc}, in accord with the analytic analysis in Sec. VI A and Eq. (34). At large separations, the relative diffusivity crosses over to power law behavior with $D_{rr} \sim r_0^{-3}$. For the packing fractions studied this crossover occurs when $r \approx 10\ \xi_{\text{struc}}$.

Increasing the colloid packing fraction has two main effects. First and most prominently, the intermediate separation regime dominated by structural correlations extends to larger separations. This results from stronger equilibrium pair correlations and is quantitatively captured by the structural decay length ξ_{struc}. Varying the packing fraction also modestly affects the overall amplitude of the correlations as normalized by the single-particle bare diffusion constant; specifically, lower volume fractions have slightly larger amplitude dynamic displacement correlations in the adopted non-dimensionalized representation.

Finally, one might wonder about the practical relevance of our large separation nonhydrodynamic power law scaling result, $D_{rr} \sim r_0^{-3}$. In the true asymptotic limit of $r_0 \to \infty$, it must become irrelevant because 3D hydrodynamics necessarily dominates given the much slower decay of correlations per Eq. (4), irregardless of any prefactor renormalization or screening issue. However, looking towards future comparisons with experiments and simulations, it becomes a delicate matter to predict at what length scale hydrodynamics does dominate. Our nonhydrodynamic power law may be relevant in an intermediate crossover regime of moderately large interparticle separations.

VII. DISCUSSION

An integrated experimental and theoretical study has been performed of the dynamic cross correlations of two tagged colloids as a function of separation and elapsed time in dense, quasi-2D layers. The measurements were done in a noninvasive manner without probe particles, and they cover a wide range of interparticle separations. The focus was on the short time regime where the large statistical data sets needed for the dynamic displacement correlation analysis can be obtained and the colloid dynamics is (largely) Fickian. Two regimes of behavior were observed. At small and intermediate separations, nontrivial structural correlations lead to an exponential decay of the dynamic correlations for the high area fraction sample, but not in the lower density suspension where nonrandom packing effects are so weak that the pair structure is essentially random. At separations sufficiently large that structure becomes randomized, apparent power law decay is observed, $D_{rr} \propto r_0^{-2.2}$, with a nearly identical amplitude for the two different area fraction samples studied.

The experimental results were quantitatively confronted with a microscopic nonhydrodynamic theory constructed based on two-particle GLE equations and a simple mode coupling approximation to treat force-force time correlations and friction. No-adjustable-parameter predictions of the theory for the dynamic cross correlations are in very good agreement with experiment over all length scales and for both suspension concentrations. The origin of the long range tail feature is due to the influence of the constraint of fixed interparticle separation on the force-force time correlation function that determines tagged particle relative and center-of-mass friction. Its spatial form is not sensitive to the presence of oscillatory pair correlations beyond contact, but its amplitude does depend on the colloids having a local hard core exclusion constraint as manifested on long length scales by a fluid dimensionless compressibility less than unity, $S(0)<1$ in Eq. (22).

The theory was also used to make testable predictions for dense 3D hard sphere fluids. The same exponential form of the dynamic cross correlation function is predicted in the structural regime. However, the long range tail decays more rapidly and without logarithmic corrections. As a consequence, the nonhydrodynamic mechanism for inducing displacement correlations is expected to be irrelevant in 3D at large separations due to a crossover to hydrodynamics-controlled behavior.

Intriguing similarities between the predictions of the prior hydrodynamic analysis [7–11] for capped monolayers and our nonhydrodynamic approach are found for quasi-2D suspensions. Similarities in key experimental features of the dynamic displacement correlations measured here and [10] are also noted. The full implications of these commonalities invite further study, not only because the physical ideas underlying the hydrodynamic and nonhydrodynamic theories are different, but also because our experiments were performed on a quasi-2D suspension with only one solid interface in contrast to the capped thin film geometry of Refs. [9–11]. For a hydrodynamics-based model this difference seems to be essential [11], in qualitative contrast to our nonhydrodynamic approach for which it is not.

A deep understanding remains to be attained for precisely why our nonhydrodynamic theory is so successful for quasi-2D suspensions. We cannot rule out that its success is tied to the different boundary conditions of our samples compared to other studies [8–11]. One might speculate that the key issues are quantitative. Specifically, as mentioned in Sec. III A, the hydrodynamic decay of displacement correlations at large separations for capped films is $D_{rr} \propto r_0^{-2}$, in contrast to the

stronger $D_{rr} \propto r_0^{-3}$ decay for two colloids near only one solid surface. The latter situation seems closer to our experimental geometry, which could imply that hydrodynamic effects are weaker than their nonhydrodynamic analog for our systems. Alternatively, in quasi-2D there may be a "near degeneracy" of how continuum hydrodynamics and nonhydrodynamical effects [Eq. (22)] determine the form of the spatial decay of displacement correlations at larger distances. In such a situation, the numerical amplitudes associated with the two different mechanisms could play a decisive role. Indeed, recall that below Eq. (22) we emphasized that the amplitude of our nonhydrodynamic mechanism differs from its hydrodynamic analog [9,10]. Given that the nonhydrodynamic mechanism accounts well for the power-law-like displacement correlations we observe at both packing fractions studied, such a scenario seems plausible as a possible reason that hydrodynamic effects can be ignored for our system. This scenario is consistent with our theoretical findings for 3D fluids. Here, the nonhydrodynamic mechanism predicts $D_{rr} \propto r_0^{-3}$ which is shorter range than in quasi-2D, in qualitative contrast to the hydrodynamic mechanism which becomes longer range in 3D, $D_{rr} \propto r_0^{-1}$, and hence is dominant at large interparticle separations.

Of course, the validity of the idea of a "near degeneracy" of mechanisms in quasi-2D may be sensitive to sample boundary conditions. Thus, it will be interesting to confront the predictions of our nonhydrodynamic theory with experiments on capped monolayers in order to better understand the subtleties of collective motion under quasi-2D confinement. In this spirit, normal mode analysis of our experimental data [37,38] may shed additional light on the role of continuum versus structural effects on relatively long distance displacement correlations.

Concerning broader implications of our work, the question of mutual correlations between moving elements in dynamically evolving structures generalizes broadly beyond colloids to systems such as polymer mixtures, biopolymer filaments at finite concentrations, intracellular environments, and other soft matter systems. Of course, quantitative aspects will depend on the specific system. Here, we considered only a sedimented quasi-2D suspension which has the practical experimental advantage of being able to be directly imaged. It serves as a model test bed in which to develop a nonhydrodynamic statistical mechanical framework and quantitatively confront it with measurements. The broader implications of our combined experimental-theoretical approach for understanding interactions between objects in close proximity are potentially powerful since under such circumstances the material cannot be considered as a featureless continuum with correlated particle dynamics determined by conventional fluid mechanics.

In the future, we plan to go beyond the current colloidal system and study how entangled biopolymer filaments diffuse when they are in close proximity such that the thermal motion of neighboring filaments induces intermolecular correlated motion. It will be interesting to discover to what extent the theoretical approach presented here might need to be substantially generalized.

From a purely theoretical perspective, the developed approach applies to any spherical particle fluid that interacts via a central pair potential at any fluid packing fraction in the short time diffusive regime. It also can be generalized to treat complex fluids composed of rigid nonspherical objects, such as the entangled biopolymers noted above. However, more work is required to treat the intermediate time regime in sufficiently concentrated systems where transient particle caging and localization leads to non-Fickian dynamics. Finally, for theorists and experimentalists alike, there remains the large challenge of integrating the hydrodynamic and nonhydrodynamic mechanisms for dynamic displacement correlations into a unified framework and dissecting their relative importance for diverse soft matter systems.

ACKNOWLEDGMENTS

This work was supported by Department of Energy, Basic Energy Science under Grant No. DE-FG02-07ER46471 administered through the Frederick Seitz Materials Research Laboratory. S.G. acknowledges office support from the Institute for Basic Science, Project Code No. IBS-R020-D1.

APPENDIX A: SINGLE-PARTICLE MEAN SQUARE DISPLACEMENT

The single-particle MSD in the nonhydrodynamic Fickian regime is [2,31]

$$\left\langle \Delta r_i^2(t) \right\rangle = 2d\ D_{(1)}^{\text{non-HD}} t. \tag{A1}$$

One can recast the diffusion constant as a friction, $D_{(1)}^{\text{non-HD}} = k_B T / \zeta_{(1)}^{\text{non-HD}}$, and calculate it from the diagonal part of the memory function [31]:

$$\zeta_{(1)}^{\text{non-HD}} = \zeta_0 + \int_0^\infty dt\ K_{(1)}(t). \tag{A2}$$

To calculate the memory function from Eq. (9b), we employ a single-particle (naive) mode coupling theory (NMCT) approach [25,26]. In NMCT, the forces are projected onto the slow bilinear density mode in Fourier space $|\rho_1(k)\rho_c(-k)\rangle$ of the single-particle and collective densities (ρ_1 and ρ_c, respectively). A standard Gaussian factorization is performed on four-point correlations. This yields the single-particle memory function [28–30]

$$K_{(1)}(t) = \frac{\rho_d}{d} \int \frac{d^d\vec{k}}{(2\pi)^d} \frac{h^2(k)}{S(k)} \Gamma_s(k,t)\, \Gamma_c(k,t), \tag{A3}$$

where all factors are defined in the main text. For consistency, we adopt the same approximations for the dynamic correlations as employed in the two-particle theory. This implies $\Gamma_s = 1$ and the collective propagator is given by Eq. (14). Using Eqs. (A2) and (A3) and performing the time integral leads to a single-particle renormalized friction

$$\frac{\zeta_{(1)}}{\zeta_0} = 1 + \frac{\rho_d}{2d} \int \frac{d^d\vec{k}}{(2\pi)^d}\, h^2(k). \tag{A4}$$

APPENDIX B: DETAILS OF TWO-PARTICLE MODE COUPLING THEORY

The two-particle MCT approach has been successfully employed in recent studies of correlated two-particle activated hopping in dense hard sphere fluids [25,26] and the relative motion of two large particles in polymer melts [27]. However, a detailed derivation of the two-particle memory function vertex

in Eq. (12) was not given in prior publications, so here we provide one in the context of the present problem.

From Eq. (9b), one has

$$K_{\alpha\beta}(t) = \frac{d}{k_B T}\left\langle f_{\alpha,i}\, f^{Q}_{\beta,i}(t)\right\rangle = \frac{d}{k_B T}\left\langle f_{\alpha,i} e^{i\hat{Q}\hat{L}t} f_{\beta,i}\right\rangle, \quad \text{(B1)}$$

where all factors are defined in the main text, and $e^{i\hat{Q}\hat{L}t}$ is the projected dynamic evolution operator. To approximately evaluate Eq. (B1), one first projects the real Newtonian forces onto the dominant slow dynamical mode of the system. The natural choice for two tagged particles in a dense fluid is a matrix projection onto the bilinear density modes $|\rho_\alpha(\vec{k})\rho_c(-\vec{k})\rangle$, where

$$\rho_\alpha(\vec{k}) = e^{i\vec{k}\cdot\vec{R}_\alpha}, \quad \text{(B2a)}$$

$$\rho_c(\vec{k}) = \sum_{\gamma\neq 1,2}^{N} e^{i\vec{k}\cdot\vec{R}_\gamma} \quad \text{(B2b)}$$

are the single tagged particle densities ($\alpha = 1,2$), and the collective density of the fluid, respectively. Then, employing a Gaussian factorization of four-point correlations, the matrix projection operator becomes

$$\hat{P} = \rho_d^{-1}\int\frac{d\vec{k}}{(2\pi)^d}\sum_{\alpha,\beta=1}^{2}|\rho_\alpha(\vec{k})\rho_c(-\vec{k})\rangle\frac{\Omega^{-1}_{\alpha\beta}(\vec{k})}{S(k)}\langle\rho_\beta(-\vec{k})\rho_c(\vec{k})|, \quad \text{(B3)}$$

where ρ_d is the d-dimensional fluid number density, $S(k)$ is the structure factor, and $\Omega^{-1}_{\alpha\gamma}$ is the matrix inverse of the static correlation matrix of the tagged particle densities:

$$\Omega_{\alpha\beta}(\vec{k}) \equiv \langle\rho_\alpha(\vec{k})\rho_\beta(-\vec{k})\rangle = \langle\exp[i\vec{k}\cdot(\vec{R}_\alpha - \vec{R}_\beta)]\rangle. \quad \text{(B4)}$$

Inserting the projection operator $\hat{P}$ on each side of the dynamic evolution operator in the force-force correlation function of Eq. (B1) then yields

$$K_{\alpha\beta} = \frac{d}{\rho_d^2 k_B T}\iint\frac{d\vec{k}\,d\vec{q}}{(2\pi)^{2d}}\sum_{\mu,\nu,\gamma,\sigma=1}^{2}\langle f_{\alpha,i}\,\rho_\mu(\vec{k})\rho_c(-\vec{k})\rangle \times\frac{\Omega^{-1}_{\mu\nu}(\vec{k})}{S(k)}\langle\rho_\nu(-\vec{k})\rho_c(\vec{k})\, e^{i\hat{Q}\hat{L}t}\rho_\gamma(\vec{q})\rho_c(-\vec{q})\rangle\frac{\Omega^{-1}_{\gamma\sigma}(\vec{q})}{S(q)} \times\langle\rho_\sigma(-\vec{q})\rho_c(\vec{q})f_{\beta,i}\rangle \quad \text{(B5)}$$

The force vertex follows from a standard calculation as [28–30]:

$$\langle f_{\alpha,i}\,\rho_\mu(\vec{k})\rho_c(-\vec{k})\rangle = -ik_i k_B T\rho h(k)\,\delta_{\alpha\mu}, \quad \text{(B6)}$$

In essence, the real forces have been replaced by effective forces determined by the equilibrium pair structure.

Further evaluation of Eq. (B6) requires additional approximations. The projected dynamics are replaced by the real dynamical evolution operator $e^{i\hat{Q}\hat{L}t} \approx e^{i\hat{L}t}$. A Gaussian factorization approximation is again employed. Equation (B5) then reduces to

$$K_{\alpha\beta} = \rho_d k_B T\int\frac{d\vec{k}}{(2\pi)^d}\sum_{\nu,\gamma=1}^{2}k_i^2 \times\frac{h^2(k)}{S^2(k)}S(\vec{k},t)\,\Omega^{-1}_{\alpha\nu}(\vec{k})\Omega_{\gamma\nu}(\vec{k},t)\,\Omega^{-1}_{\gamma\beta}(\vec{k}), \quad \text{(B7)}$$

where $S(k,t) \equiv S(k)\Gamma_c(k,t)$ with $\Gamma_c(k,t)$ given by Eq. (14) of the main text, and $\Omega_{\gamma\nu}(\vec{k},t)$ is the time-dependent tagged particle density-density correlation function, which is the dynamic equivalent of Eq. (B4). For the latter, we employ the following approximation:

$$\begin{aligned}\Omega_{\gamma\nu}(\vec{k},t) &\equiv \langle e^{i\vec{k}\cdot(\vec{r}_\gamma(0)-\vec{r}_\nu(t))}\rangle = \langle e^{i\vec{k}\cdot[\vec{r}_\gamma(0)-\vec{r}_\nu(0)]}\cdot e^{i\vec{k}\cdot[\vec{r}_\nu(0)-\vec{r}_\nu(t)]}\rangle\\ &\approx \langle e^{i\vec{k}\cdot[r_\gamma(0)-\vec{r}_\nu(0)]}\rangle\langle e^{i\vec{k}\cdot[\vec{r}_\nu(0)-\vec{r}_\nu(t)]}\rangle = \Omega_{\gamma\nu}(k)\Gamma_s(k,t)\\ &\approx \Omega_{\gamma\nu}(k). \end{aligned} \quad \text{(B8)}$$

The factorization on the second line decouples static two-particle correlations from single-particle motion in the spirit of a Vineyard approach [35]. The final result ignores the effect of tagged particle self-diffusion on memory function relaxation. This approximation is in the spirit of assuming that the collective dynamics of the fluid surrounding the tagged particles dominates force memory relaxation for dense fluids at short times, an idea employed in the main text and Appendix A. The arguments leading to these simplifications justify why we have not done a full self-consistent solution of the MCT equations associated with the two tagged particles, and are consistent with our focus on short time Fickian dynamics of the cross correlations.

Using all the above approximations in Eq. (B7), and collapsing the resulting sums using the static matrix inverse identity, yields

$$K_{\alpha\beta} = \frac{\rho_d k_B T}{d}\int\frac{d\vec{k}}{(2\pi)^d}k_i^2\frac{h^2(k)}{S(k)}\Gamma_s(\vec{k},t)\Gamma_c(\vec{k},t)\,\Omega^{-1}_{\alpha\beta}(\vec{k}). \quad \text{(B9)}$$

To derive Eq. (8) in the main text, one then calculates the matrix inverse of Eq. (B4). Recall that $\Omega_{\alpha\beta}$ depends only on the separation of the two particles $r = |\vec{r}_\alpha - \vec{r}_\beta|$, and hence

$$\Omega_{\alpha\beta}(k) = \begin{pmatrix}1 & \omega_{12}(k)\\ \omega_{12}(k) & 1\end{pmatrix}, \quad \text{(B10)}$$

where $\omega_{12}(k)$ is the constraint function discussed in the main text. Inverting this matrix, employing the definition of the center-of-mass and relative memory functions [defined below Eq. (10)], and using all the above results, we then obtain Eq. (12). Note that the constraint of fixed interparticle separation enters only through the matrix inverse of Eq. (B10), which is mathematically analogous to the influence of bonding on force time correlations for a diatomic molecule [39,40].

[1] R. Brown, Philos. Mag. **4**, 161 (1828).

[2] J. P. Hansen and I. R. McDonald, *Theory of Simple Liquids* (Academic, London, 1986).

[3] T. M. Squires and T. G. Mason, Annu. Rev. Fluid Mech. **42**, 413 (2010).

[4] J. C. Crocker, M. T. Valentine, E. R. Weeks, T. Gisler, P. D. Kaplan, A. G. Yodh, and D. A. Weitz, Phys. Rev. Lett. **85**, 888 (2000).

[5] L. Starrs and P. Bartlett, J. Phys.: Condens. Matter **15**, S251 (2003).

[6] A. J. Levine and T. C. Lubensky, Phys. Rev. E **65**, 011501 (2001).
[7] E. R. Dufresne, T. M. Squires, M. P. Brenner, and D. G. Grier, Phys. Rev. Lett. **85**, 3317 (2000).
[8] W. Zhang, S. Chen, N. Li, J. Z. Zhang, and W. Chen, PLoS ONE **9**, e85173 (2014).
[9] A. Marcus, J. H. Schofield, and S. A. Rice, Phys. Rev. E **60**, 5725 (1999).
[10] H. Diamant, B. Cui, B. Lin, and S. Rice, J. Phys.: Condens. Matter **17**, S4047 (2005).
[11] B. Lin, B. Cui, X. Xu, R. Zangi, H. Diamant and S. A. Rice, Phys. Rev. E **89**, 022303 (2014).
[12] E. E. Ballard and A. L. Kholodenko, Physica A **388**, 3024 (2009).
[13] C. Beenakker and P. Mazur, Phys. Lett. A **98**, 22 (1983).
[14] C. Beenakker and P. Mazur, Physica A **126**, 349 (1984).
[15] V. Pryamitsyn and V. Ganesan, J. Chem. Phys. **128**, 134901 (2008).
[16] M. Muthukumar and S. Edwards, Macromolecules **16**, 1475 (1983).
[17] T. Ando, E. Chow, and J. Skolnick, J. Chem. Phys. **139**, 121922 (2013).
[18] D. O. Riese, G. H. Wegdam, W. L. Vos, R. Sprik, D. Fenistein, J. H. H. Bongaerts, and G. Grübel, Phys. Rev. Lett. **85**, 5460 (2000).
[19] K. F. Freed and M. Muthukumar, J. Chem. Phys. **68**, 2088 (1978).
[20] L. Durlofsky and J. Brady, Phys. Fluids **30**, 3329 (1987).
[21] J. Pesic, J. Z. Terdik, X. Xu, Y. Tian, A. Lopez, S. A. Rice, A. R. Dinner, and N. F. Scherer, Phys. Rev. E **86**, 031403 (2012).
[22] J. Deutch and I. Oppenheim, J. Chem. Phys. **54**, 3547 (1971).
[23] G. T. Evans and D. Kivelson, J. Chem. Phys. **85**, 7301 (1986).
[24] M. Guenza, J. Chem. Phys. **110**, 7574 (1999).
[25] D. M. Sussman and K. S. Schweizer, J. Chem. Phys. **134**, 064516 (2011).
[26] D. M. Sussman and K. S. Schweizer, Phys. Rev. E **85**, 061504 (2012).
[27] U. Yamamoto and K. S. Schweizer, J. Chem. Phys. **139**, 064907 (2013).
[28] W. Gotze and L. Sjogren, Rep. Prog. Phys. **55**, 241 (1992).
[29] W. Gotze, *Complex Dynamics of Glass-Forming Liquids: A Mode-Coupling Theory* (Oxford University Press, New York, 2008).
[30] T. R. Kirkpatrick and P. G. Wolynes, Phys. Rev. A **35**, 3072 (1987)
[31] R. Zwanzig, *Nonequilibrium Statistical Mechanics* (Oxford University Press, New York, 2001).
[32] M. Doi and S. F. Edwards, *The Theory of Polymer Dynamics* (Clarendon, Oxford, 1986).
[33] S. I. Doguwa, Biometrical J. **32**, 95 (1990).
[34] P. G. deGennes, Physica **25**, 825 (1959).
[35] G. H. Vineyard, Phys. Rev. **110**, 999 (1958).
[36] A. Santos, M. L. de Haro, and S. B. Yuste, J. Chem. Phys. **103**, 4622 (1995).
[37] R. Zangi and S. A. Rice, J. Phys. Chem. B, **108**, 6856 (2004).
[38] P. J. Yunker, K. Chen, M. D. Gratale, M. A. Lohr, T. Still, and A. G. Yodh, Rep. Prog. Phys. **77**, 056601 (2014).
[39] R. Zhang and K. S. Schweizer, Phys. Rev. E **80**, 011502 (2009).
[40] K. S. Schweizer, J. Chem. Phys. **91**, 5802 (1989).